

Received 6 June 2023, accepted 26 June 2023, date of publication 7 July 2023, date of current version 26 July 2023.

Digital Object Identifier 10.1109/ACCESS.2023.3293090

## APPLIED RESEARCH

# Coronary Artery Segmentation Based on Transfer Learning and UNet Architecture on Computed Tomography Coronary Angiography Images

BELÉN SERRANO-ANTÓN<sup>1,2,3</sup>, ALBERTO OTERO-CACHO<sup>1,2,3</sup>, DIEGO LÓPEZ-OTERO<sup>4,5</sup>,  
BRAIS DÍAZ-FERNÁNDEZ<sup>4,5</sup>, MARÍA BASTOS-FERNÁNDEZ<sup>4,5</sup>,  
VICENTE PÉREZ-MUÑUZURI<sup>3,6</sup>, JOSÉ RAMÓN GONZÁLEZ-JUANATEY<sup>4,5</sup>,  
AND ALBERTO P. MUÑUZURI<sup>2,3</sup>

<sup>1</sup>FlowReserve Labs S.L., 15782 Santiago de Compostela, Spain

<sup>2</sup>CITMAga, 15782 Santiago de Compostela, Spain

<sup>3</sup>Group of Nonlinear Physics, University of Santiago de Compostela, 15782 Santiago de Compostela, Spain

<sup>4</sup>Cardiology and Intensive Cardiac Care Department, Hospital Clínico Universitario de Santiago de Compostela, 15706 Santiago de Compostela, Spain

<sup>5</sup>Centro de Investigación Biomédica en Red de Enfermedades Cardiovasculares (CIBERCV), 28029 Madrid, Spain

<sup>6</sup>Institute CRETUS, Group of Nonlinear Physics, University of Santiago de Compostela, 15705 Santiago de Compostela, Spain

Corresponding author: Alberto Otero-Cacho (alberto.otero@flowreserve.es)

This work was supported in part by Spanish Ministerio de Economía y Competitividad and European Regional Development Fund under Contract RTI2018-097063-B-I00 AEI/FEDER, UE; in part by Xunta de Galicia under Grant 2021-PG036; in part by Spanish Ministerio de Ciencia e Innovación MCIN/AEI/10.13039/501100011033 through the Industrial Doctorates Grant and European Union NextGenerationEU/PRTR Research under Grant DIN2020-011068; and in part by FEDER (UE).

This work involved human subjects or animals in its research. Approval of all ethical and experimental procedures and protocols was granted by the Research Ethics Committee Santiago-lugo.

**ABSTRACT** Coronary artery segmentation from CT scans is a helpful tool for coronary artery diseases diagnosis, which is frequently characterised by a vessel narrowing (stenosis). This is a highly demanded and high time-consuming process, thus automated procedures are becoming increasingly necessary. In this work, we propose an extremely light computationally 2D UNet that uses transfer learning for the first time in CT images. We compare the results, using different architectures and backbones, of a 2D UNet and a 3D UNet trained from scratch (i.e. weights are randomly initialised) and a 2D EfficientUNet. Both the amount of input data, with a total of 88 patients, and the extension of the structure to be recognised, the aorta and the coronary arteries ( $A + C.A$ ), as well as the coronary arteries only ( $C.A$ ) are analysed. Network outputs in clinically identified stenotic lesion areas are also assessed. The results show the advantage of using transfer learning when data is scarce, improving the  $F_1$  score by up to 0.6 points for the 2D UNet. On the other hand, when data is sufficient,  $F_1$  score values are close to 0.9 for all the networks. Besides, the results reveal that the 2D UNet distinguishes the thinnest and most distal vessels, although in the presence of a lesion, there is a clear tendency to overestimate it. The network with the best accuracy is the 3D UNet, with values above 95% and 75% in  $A + C.A$  and  $C.A$ , respectively. Moreover, the proposed methods show dependence on the amount of training data and dataset structure ( $A + C.A$  or  $C.A$ ).

**INDEX TERMS** Artery, convolutional neural network, coronary, CT, segmentation, UNet.

## I. INTRODUCTION

Coronary artery disease (CAD) is one of the leading causes of death worldwide [1], [2]. Invasive tests, such as coronary

The associate editor coordinating the review of this manuscript and approving it for publication was Juan A. Lara.

angiography, with high spatial resolution and the possibility of intervening in the same procedure, can be used to diagnose this disease. However, due to the associated risks, non-invasive techniques such as computed tomography (CT) are increasingly being employed [3]. Coronary computed tomography angiography (CCTA) allows the extraction of

images of the heart in slices. If a contrast agent (dye) is used, these images show whether the arteries are narrowed or not. Additionally, each scan can be integrated to create a 3D visualization that greatly aids diagnosis. After the images are taken, lesions are visually assessed by an expert. Nonetheless, this is a tedious, error-prone, subjective and time-consuming process.

One of the solutions to speed up the process and obtain an accurate diagnosis is to obtain a precise 3D geometry of the region of interest (aorta and coronary arteries). This enables not only the visualisation of the structure but also the calculation of other clinically-relevant diagnostic parameters such as Fractional Flow Reserve (FFR), using computational fluid dynamics or machine learning techniques [4], [5], [6], [7].

Semi-automatic and automatic segmentation (pixel-by-pixel identification of structures) techniques are used to obtain these geometries. Although semi-automated techniques involve many tools, such as threshold structure filtering on Hounsfield units, centerline extraction, or 3D editing, they still require time and expertise. In automatic segmentation techniques, artificial intelligence (AI) is increasingly being applied, for example Convolutional Neural Networks (CNN) [8], [9]. The main advantage of these methods is that they are not user-dependent and can therefore be used by both expert personnel and personnel from areas outside the field of medical imaging. This is helpful for research and reproducibility of results, as well as saving a lot of time.

Within the architectures described by CNN, UNet has played a relevant role in biological image segmentation [10]. This type of network consists of two parts: an encoder that reduces the spatial dimension of each layer and increases the number of channels, and a decoder that performs the reverse process. Some modifications of this architecture can be found in the literature in the field of coronary structure segmentation, such as 3D versions of UNet itself (3D UNet), VNet or UNet++ [11], [12], [13], [14], [15], [16].

Cheung et al. [12] propose a modified and computationally cheap 2D UNet that obtains a dice similarity coefficient (DSC) [17] of 91.20% and 88.8% when trained with the entire coronary tree (aorta and coronary arteries) and with the coronary arteries, respectively. Their dataset consists of 71 CT scans. Other works such as [13], propose a computationally intensive model based on 3D UNet with a dataset of 474 CT scans. In this case, the DSC in the coronary arteries increased to 96.91%. Huang et al. [14] use a 3D UNet with two settings, depending on whether the data include vessel centerlines (18 CCTA) or not (34 CCTA). Duan et al. [18] suggests a 3D UNet with prior spatial knowledge of coronary geometries, which allows to reduce the complexity of the model.

The DSC received here is 71.46%. On the other hand, Gu and Cai [15] combine the advantages of 2D UNet (wide field of view) and 3D (its ability to favor structural continuity) in a 2D-3D UNet network. This implementation achieves a

DSC of 97.54% in aorta and 86.62% in coronary arteries. This method achieves a DSC of 79.5% in the coronary arteries.

An additional benefit of CNNs is their simplicity to transfer learning. This is particularly intriguing when the quantity of labeled data, time and assets are restricted [19]. It is not business as usual, consequently, that transfer learning procedure has been applied to clinical imaging and, specifically, to coronary artery and atherosclerotic plaque segmentation [20]. For example, [21] utilizes a pre-trained (VGG16, ResNet50, and Inception-v3) CNN for stenosis region location in coronary angiography through transfer learning and fine tuning of a synthetic dataset of 10,000 pictures tested with various setups. With the best design, they got a  $F_1$  score of 0.98. Candemir et al. [22] additionally features the benefits of utilising transfer learning in architectures, for example, VGG-16 [23], particularly when the dataset is small, as their weights have been optimised through more than one million pictures from ImageNet [24]. In any case, they additionally bring up the absence of pre-trained 3D networks.

All the articles mentioned above, including this one, face some problems with respect to coronary artery segmentation. 1) Data scarcity. The results obtained by neural networks depend, to a large extent, on the input data. In the case of coronary artery segmentation, images are difficult to obtain (as they are clinical data) and require a previous manual segmentation. 2) The datasets obtained are class imbalanced, as the coronary vessels constitute a very small region within each slice. 3) Some approaches such as 3D networks are computationally very intensive, either in terms of memory or in computation time.

The main contributions of the present study are:

- 1) Study of the dependence of the number of patients for obtaining an accurate coronary tree with UNet neural networks.
- 2) Comparison of 2D (with different backbones) and 3D networks. As a novelty to previous studies, transfer learning in 2D is included.
- 3) Training with a very detailed and accurate dataset.

This article is structured as follows. Section II describes the methods, including image acquisition, dataset processing and technical specifications of the algorithms. Section III details the performance of the algorithms and shows examples of the volumes obtained. Finally, section IV contains the discussion and conclusions.

## II. METHODS

### A. CLINICAL DATA AND PRE-PROCESSING

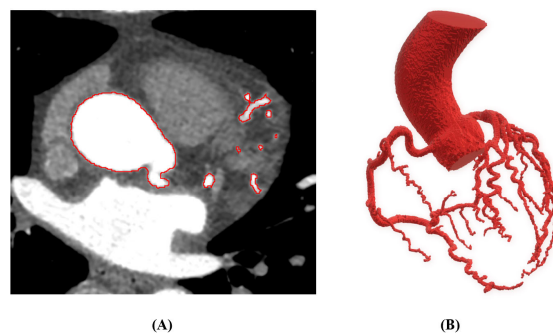
The dataset used for this study contains CT images from 88 patients that have been obtained at the University Hospital in Santiago de Compostela (Spain). CCTA is obtained for each patient consisting of 256 images with a 512x512 pixel resolution. Patients were chosen based on a clear image criterion and the lack of calcium-related lesions. If a patient develops some calcification (less than 5% of the patients), the calcium is washed out of the vessel, while maintaining

the blood flow region. CCTA images were obtained using a Revolution CT [25], with a one-beat 16cm wide coverage and 0.23mm spatial resolution. Acquisition parameters and patient premedication were chosen following the Society of Cardiovascular Computed Tomography recommendations.

The images were cropped to a size of 400x400 pixels in order to reduce their size and non-essential information. The amount of the images per patient was also decreased from 256 to 200. Note that the quality of the images was never decreased and neither the aorta nor any other coronary structures of importance were eliminated. The Hounsfield Units used to measure the pixel intensity have been rescaled to yield values between 0 and 255.

### B. ETHICS STATEMENT

The development of the project was carried out respecting the Declaration of Helsinki of the World Medical Association 1964 and ratifications of the following assemblies (Tokyo 75, Venice 83, Hong Kong 89, Somerset West 96, Scotland 00, Seoul 08 and Fortaleza 13) on ethical principles for medical research on human beings, RD 1090/2015, of December 24, on clinical trials, specifically the provisions of article 38 on good clinical practices, and the Convention on human rights and biomedicine, made in Oviedo on April 4, 1997 and successive updates. The researchers participating in this study agree that all clinical data collected from the study subjects will be separated from personal identification data ensuring the anonymity of the patient; respecting the Personal Data Protection Law (Organic Law 15/1999, of December 13), RD 1720/2007 of December 21, which approves the Regulations for the development of Organic Law 15/1999, Law 41/2002, of November 14 (basic regulation of patient autonomy and rights and obligations in terms of information and clinical documentation), as well as Law 3/2001, of May 28, (regulator of informed consent and the clinical history of patients), Law 3/2005, of March 7, modifying Law 3/2001 and Decree 29/2009 of February 5, which regulates access to history electronic clinic. The clinical data of the patients will be collected by the investigator in the Case Report Form (CRF) specific to the study. Each CRF will be encrypted, protecting the identity of the patient. Only the research team and the health authorities, who have a duty to maintain confidentiality, will have access to all the data collected for the study. Only information that cannot be identified may be transmitted to third parties. Once the study is finished, the data will be destroyed. The treatment, communication and transfer of data will be done in accordance with the provisions of the General Data Protection Regulation (Regulation (EU) 2016/679 of the European Parliament and of the Council, of April 27, 2016). The data collected will only be used for the purposes of the research study described in the protocol and kept for the time necessary to achieve the objectives of the study and in accordance with applicable legislation. As this is a retrospective study of medical records and archived samples that does not deviate from routine clinical practice, the Ethics Committee consider



**FIGURE 1.** Example of patient segmentation. A) Slices of the CT image with the segmentation line of the aorta and the coronary arteries in red. B) 3D geometry of the coronary tree obtained from the slices.

that patient informed consent and fully anonymization of the data before being access are sufficient requirements to carry out the study.

### C. GROUND TRUTH SEGMENTATION

The process to obtain ground truth labels was carried out semi-automatically with 3D Slicer software (version 4.11.20210226) [26], [27]. The task was designed in three steps: 1) thresholding, 2) cleaning and 3) refinement.

- 1) Thresholding: A threshold is established to extract coronary structures with good contrast. During this process not only the aorta and coronary arteries are segmented, but also other parts of the muscle or ventricles.
- 2) Cleaning: From the previous step, structures other than the aorta or coronary arteries are removed.
- 3) Refinement: Narrow and distal vessels are segmented by thresholds lower than in step 1).

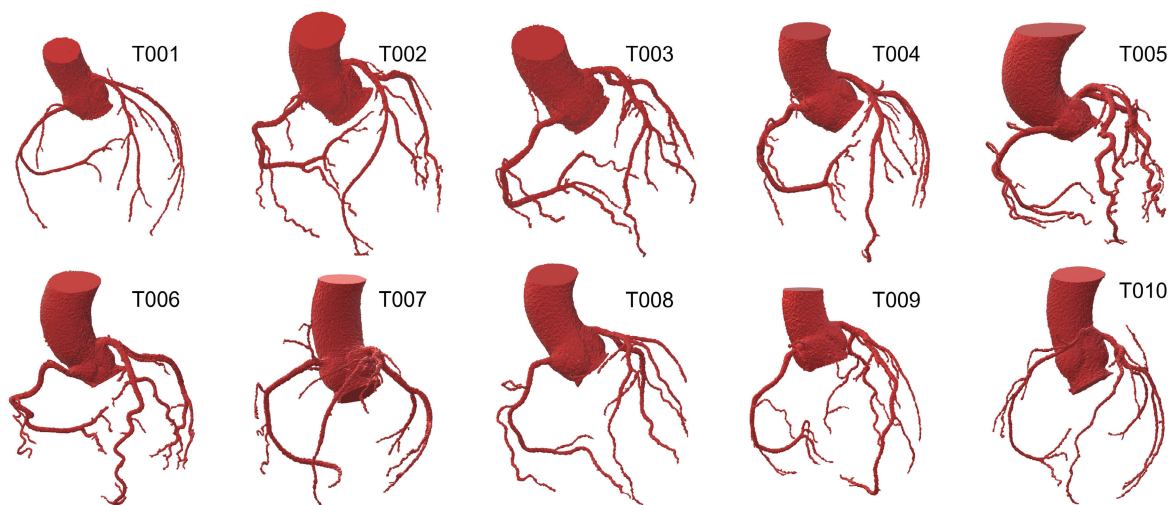
The refinement step distinguishes our study from previous works as it performs a thorough segmentation of the entire coronary tree (see Fig. 1). Once the aorta and coronary arteries have been segmented, the aorta is removed, leaving only the coronary arteries to generate the two study datasets. One with the complete structure and the other set with only the coronary arteries.

Finally, the volume is downsized to 200x400x400 and a binary mask is applied to obtain the ground truth labels (GT).

### D. METHOD

#### 1) MODEL

The UNet architecture underlies the models we compare. The first model is a 2D UNet. The peculiarity of this network is that it has an encoder that has already been trained through more than one million pictures from ImageNet [24] and whose weights cannot be changed, as well as a decoder that can be trained. The encoder is based on *MobileNetV2* [28] and is already implemented in *tensorflow.keras.applications* [29] (see model2Dpre.json file in Supplementary Material). This network was chosen because of its low computational cost and high performance. It is 32 times smaller and 27 times less computationally



**FIGURE 2.** Segmentation ground truth (GT) of the 10 test patients.

intensive than VGG16 while maintaining competitive accuracy [28].

Furthermore, by using a pre-trained encoder and keeping these weights constant, the number of variable parameters can be significantly reduced. In this case, the total number of parameters is 6,502,786, of which 4,658,882 are trainable and 1,843,904 are non-trainable. Because the input size in the first implementation of this network is fixed at 512x512, the 400x400 images of our dataset are filled with a black frame until the required size is obtained. This allows us to use the same dataset for both 2D and 3D algorithms.

A 3D UNet is the second model. The input and output of this network are volumes made up of 16 images (CCTA slides). Following the implementation of [13], each 16-image patch contains information from the previous and next patch. This network has a total of 22,575,329 trainable parameters.

The complete architecture of both models is in the Supplementary Material in Fig. S1 and Fig. S2. In addition, a diagram of the 3D UNet is shown in Fig. S3.

## 2) COMPARISON WITH OTHER NETWORKS

To strengthen the study, the results of the pre-trained 2D UNet and the 3D UNet are compared with a 2D UNet, whose weights are randomly initialised (in what follows we will refer to it as “from scratch”), and a pre-trained 2D UNet but with a different backbone, in this case an EfficientUNet [30]. Like the 2D pre-trained UNet, this network has also been pre-trained with the ImageNet dataset [24] and only the decoder is trained.

The random initialised 2D network consists of 7,760,322 parameters and details of its architecture can be found in Supplementary Material, Fig. S4.

Furthermore, the architecture and implementation of the EfficientUNet is based on a *efficientnetb5* whose original code and information about its implementation can be found in [31].

The training datasets are exactly the same as for the 2D pre-trained UNet and 3D UNet, so an “apple to apple” comparison can be made.

## 3) TRAINING

One goal of this work is to determine the relationship between the amount of data (in this case, patients) and the segmentation results. Patients were divided into training, validation, and test sets to achieve this goal, following train-test split strategy. The test set consists of 10 patients whose segmentation (ground truth (GT)) can be seen in Fig. 2. The number of training patients,  $N$ , increases in steps of 10 in the range [15, 65], and the number of patients in the validation set corresponds to 20% of  $N$ . That is, if  $N = 55$ , there are  $55 * 0.2 = 11$  patients in the validation set. The same is true for both  $A + C.A$  and  $C.A$ . Such studies are not commonly found in the literature, however, they allow to gain intuition about the number of data needed to obtain quality coronary geometries. This is especially important when dealing with hard-to-obtain data, such as clinical data.

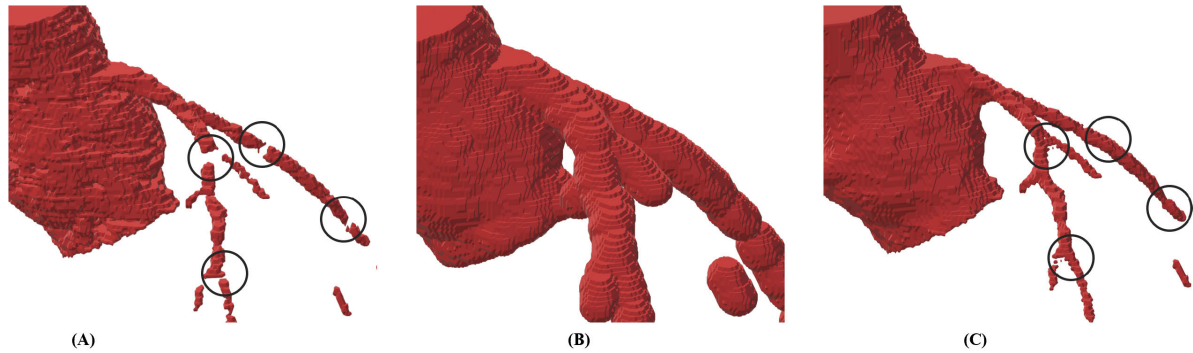
In the case of 2D UNet from scratch and 2D EfficientUNet  $N = 15$  and  $N = 65$  was considered, since its implementation is intended only for comparison purposes.

## 4) IMPLEMENTATION

The implementation of the models is developed in Python (v 3.7) [32], [33] and Tensorflow Keras API (v 2.6-tf) [29], [34]. The loss function we used for the study is binary cross entropy [34], [35], [36].

The problem of class imbalance has been tackled by giving five times more weight to the vessel class than to the background class, weighted cross entropy (focal loss). For the optimisation of the models, the Adam algorithm [34], [37] has been used. Convolutional kernel size is set to 3. A MaxPooling layer follows the convolutional layer with a stride of 2 and its followed by a ReLU activation function for





**FIGURE 3.** Example grow-shrink algorithm. A) Result segmentation from UNet. B) Grow step. C) Shrink step.

both 2D and 3D networks. All information about the networks structure can be found in Section S.I in Supplementary Material.

Each training consists of 50 epochs. In order to avoid overfitting, Early Stopping is used with *patience* = 5 and *monitor* = *val\_loss* (loss function evaluated on the validation set).

#### E. POST-PROCESSING

Two algorithms were used to generate cleaner and more connected structures. The first of them is based on the removal of components not connected to the main structure (islands) with values less than 50 voxels. This method will be referred to as *I* in the following. Grow-shrink algorithm, on the other hand, is applied with a width of 2mm (see Fig. 3). Throughout the text, this method will be referred to as *G*. These algorithms were applied sequentially in both *I*-*G*) and *G*-*I*) orders.

#### F. EVALUATION METRICS

The fit goodness of the networks considered was evaluated, and, for that, 10 test patients were chosen (see Fig. 2). It should be noted that their manual segmentation is extremely detailed (very thin and distal vessels are included). Furthermore, due to variations in image contrast and the shape of the coronary artery tree, this test set is heterogeneous in terms of geometric complexity.

The parameters chosen for the evaluation are well known in the field of segmentation. These include true positives (TP), false positives (FP), true negatives (TN) and false negatives (FN). The following indicators were defined based on these [17], [38]:

- Precision:  $TP/(TP + FP)$ .
- Recall:  $TP/(TP + FN)$ .
- $F_1$  score or dice similarity coefficient (DSC): is the harmonic mean of precision and recall ( $TP/(TP + 0.5 * (FP + FN))$ ). It can also be expressed as  $2 * (Y \cap \hat{Y})/(|Y| + |\hat{Y}|)$ . Where  $Y$  and  $\hat{Y}$  represent ground truth and prediction, respectively, and  $Y, \hat{Y} \in \{0, 1\}$ .
- $F_1^a$  score ( $F_1$  score attached): since we found false positives isolated from the coronary structure in the results, we define this  $F_1^a$  score in the same way as  $F_1$  but

only taking into account those FPs that are in contact with a TP. This quantifies how difficult it is to clean the final result of the network if we want to obtain a coronary tree without external structures. Moreover, it is an indicator of oversizing, which is critical if the purpose of coronary geometry is to calculate clinical parameters such as FFR [5].

Another requirement for clinical use of the network-predicted geometries is that the entire geometry is composed by only one connected component (CC). As a consequence, the number of connected components in the coronary regions of interest is also calculated.

To complete the statistical study and visualise the performance of the networks, Bland-Altman plots are included for the area of the coronary geometry in each axial slice of the volume (see Fig. S20 to Fig. S23 in Supplementary Material).

#### G. LESION EVALUATION

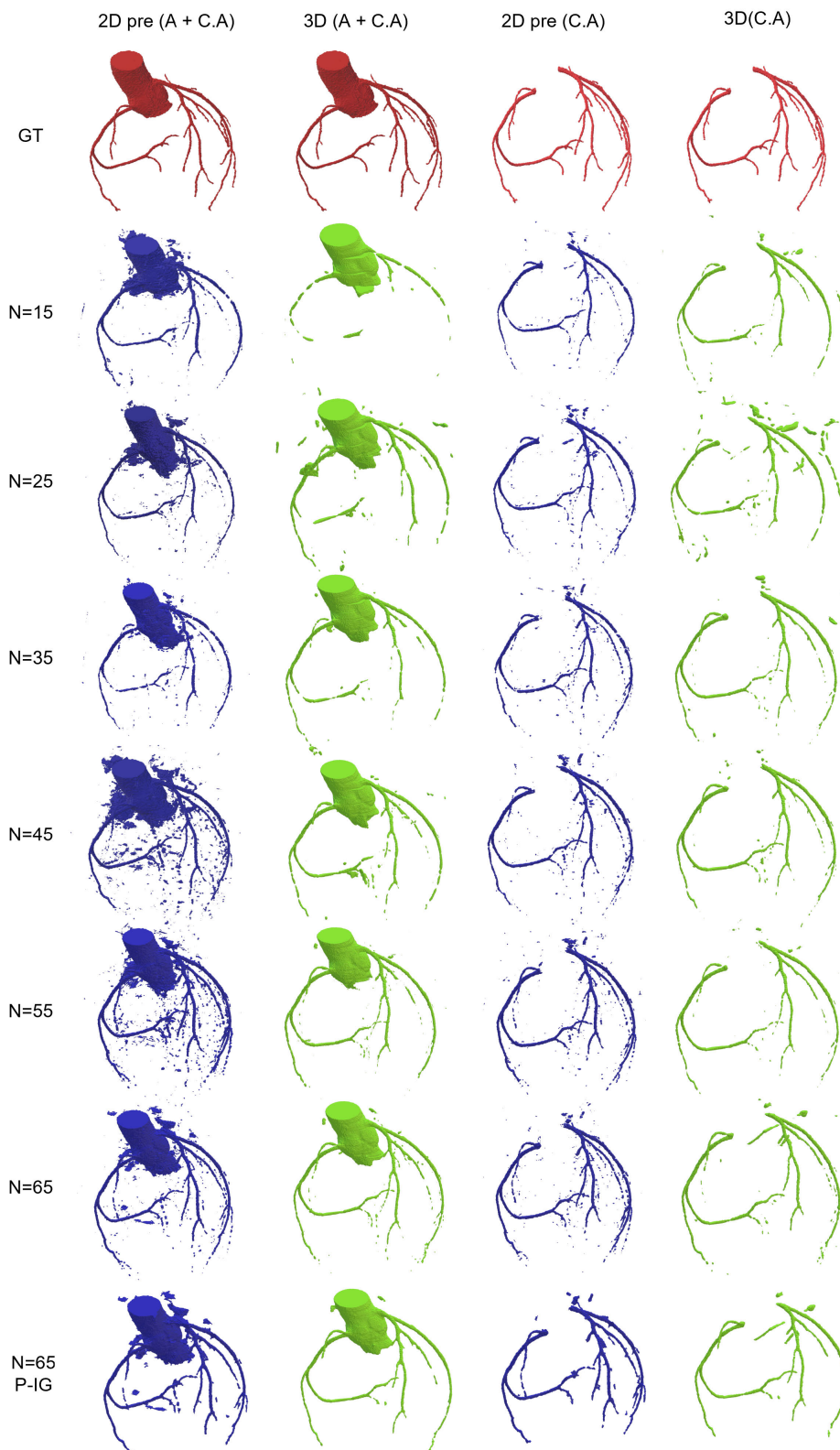
This work includes an evaluation of the network prediction in two stenosis diagnosed as severe by clinicians. This is critical because the network's accuracy should improve in the lesion-affected regions.

This assessment compares the segmentation performed by an expert (ground truth (GT)) to that predicted by the network from a geometrical standpoint. Although other papers, such as [39], assess lesions using the  $F_1$  score, a geometric and visual assessment was preferred in this case because it is more informative than the  $F_1$  score since over/undersized areas can be seen and measured. The volume at the intersection and the difference in the lesion region are provided, as well as their graphical representation.

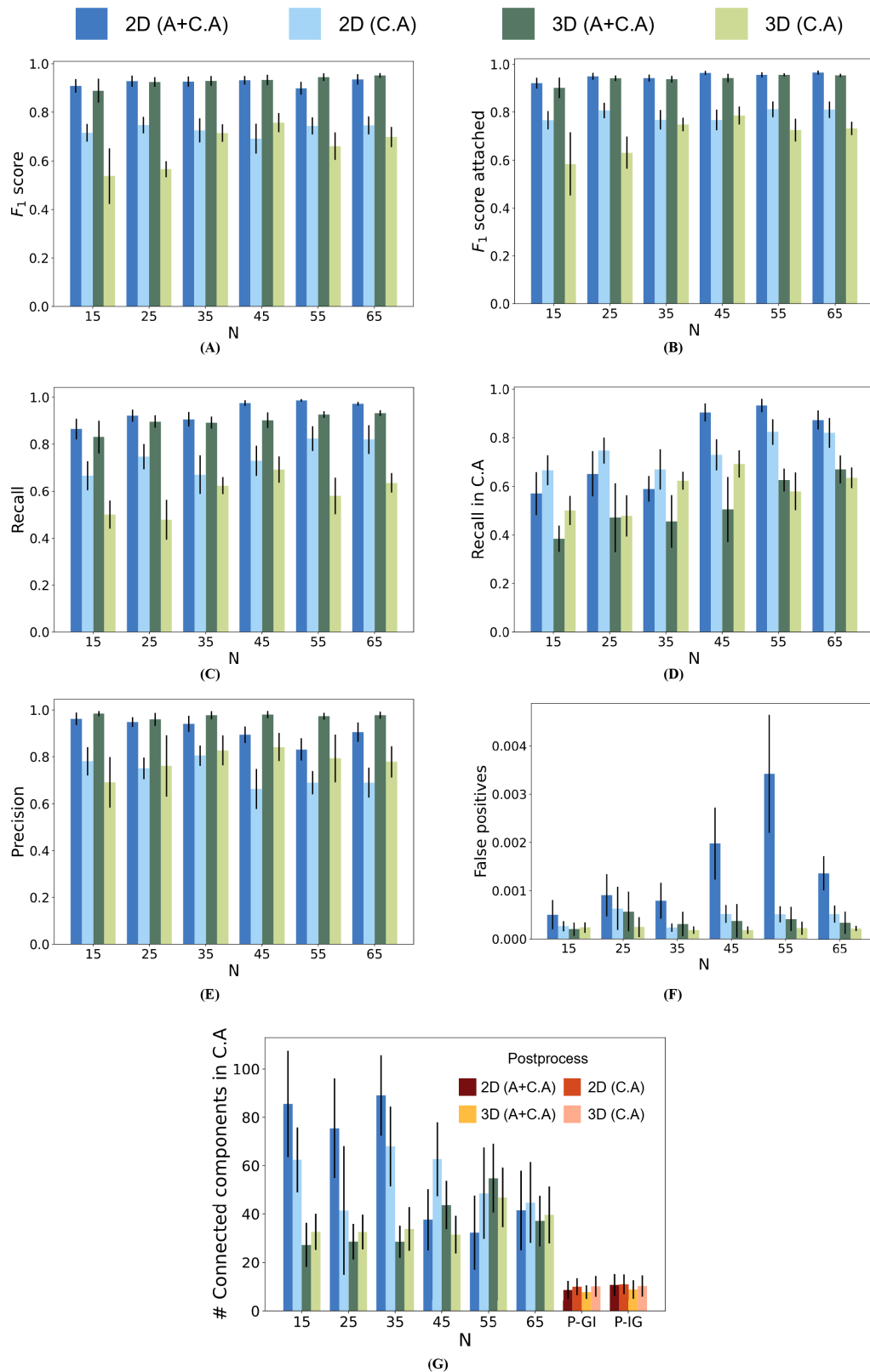
### III. RESULTS

#### A. GEOMETRY PREDICTION

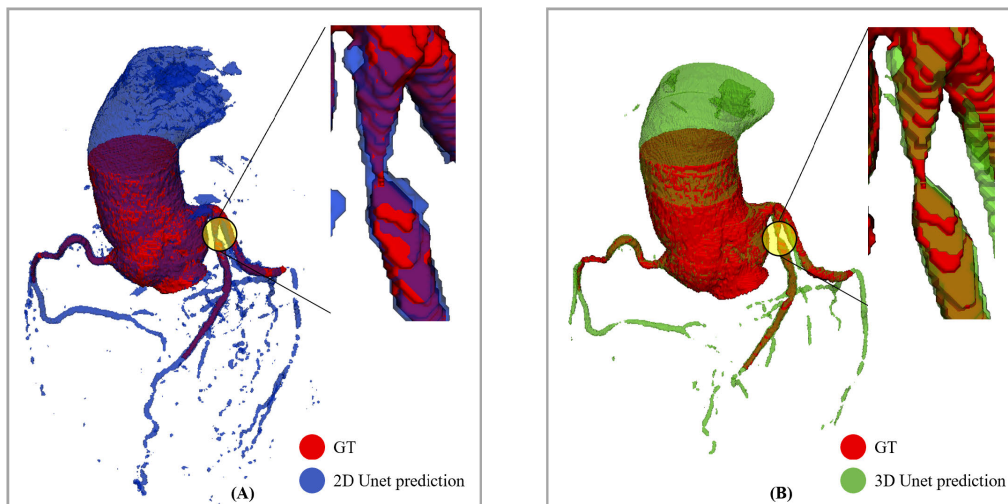
The network segmentation for test patient T001 is shown in Fig. 4. It depicts how the outcomes change as the number of training patients grows. In the instance of the 2D UNet, it is clear that vessel detection improves while false positives grow. The 3D UNet, on the other hand, starts with sliced and basic segmentations and ends up recognising all of the major vessels while keeping a cleaner segmentation.



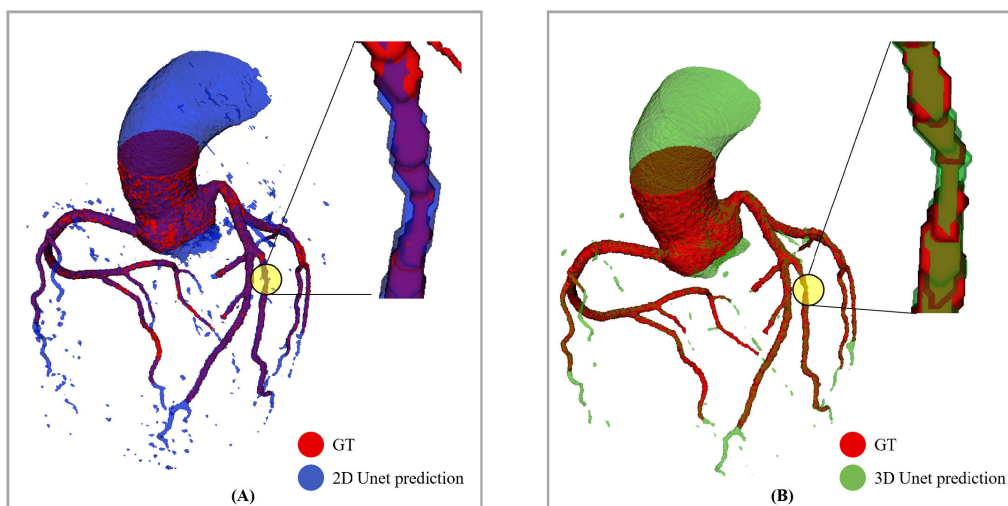
**FIGURE 4.** Example of predicted segmentations carried out by 2D UNet pre-trained and 3D UNet for test patient T001 on aorta and coronary arteries (A + C.A) and coronary arteries only (C.A). Datasets were trained with different number of patients (N). The validation set consisted of 20% of N. The last row shows the results obtained after post-processing the image using the IG algorithm (first the small islands are removed and then grow-shrink is applied).



**FIGURE 5.** Parameter values of 2D UNet pre-trained and 3D UNet results on aorta and coronary arteries (A + C.A) and coronary arteries only (C.A) datasets. The X-axis shows the number of patients used for the training set ( $N$ ). On the Y-axis, the value of the corresponding parameter. A)  $F_1$  score. B)  $F_1^a$  score. C) Recall. D) Recall in coronary arteries. E) Precision. F) False positive to background class number of pixels ratio. G) Number of connected components in coronary arteries.



**FIGURE 6.** Segmentations of the coronary tree of Lesion 1. In red the manual segmentation performed by an expert. (A) In blue the prediction performed by the 2D pretrained UNet,  $N = 65$ . (B) In green the prediction of the 3D UNet,  $N = 65$ . The zoomed-in part shows the region of the lesion.



**FIGURE 7.** Segmentations of the coronary tree of Lesion 2. In red the manual segmentation performed by an expert. (A) In blue the prediction performed by the 2D pretrained UNet,  $N = 65$ . (B) In green the prediction of the 3D UNet,  $N = 65$ . The zoomed-in part shows the lesion region.

In addition, the segmentation for test patient T003 can be seen in Supplementary Material (Fig. S5). Furthermore, the last row shows the effect of post-processing. Structures become cleaner and more connected while maintaining the quality of the previously segmented vessels.

Fig. 5 shows the parameter values achieved for each type of network and training. Errorbars with mean and standard deviation represent the outcomes of the 10 test patients from 3 trainings with different data (all with the same number of patients,  $N$ ), for a total of 30 values (see csv file in Supplementary Material).

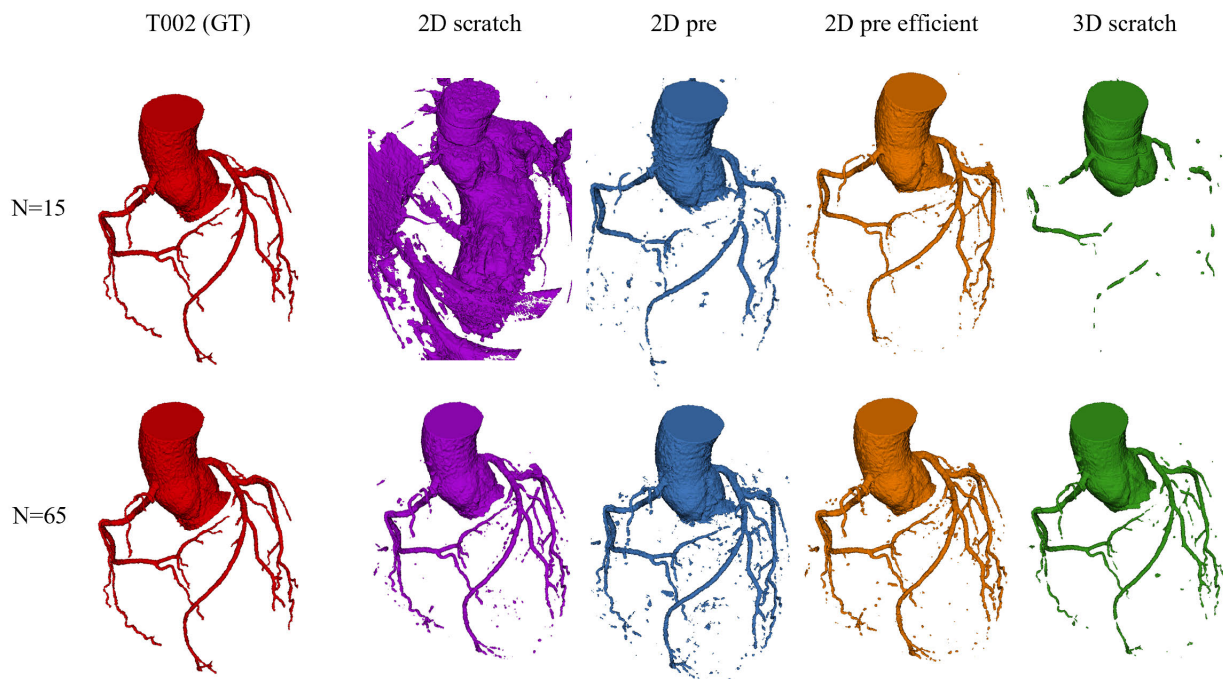
The first parameter to be addressed is the  $F_1$  score, which is presented in Fig. 5.A. This is an indicator, in the range [0, 1], of the similarity between two binary masks, where 0 implies no match between the two masks and 1 a full match. In a binary case, such as ours, it is equivalent to the DSC [17].

One item that strikes out are the numbers for  $A + C.A$  training that are around 0.9 and fluctuate slightly with  $N$ . This is because the aorta takes up a considerable portion of the volume and is a structure that both networks recognise. In particular, we always get numbers in the range [0.89, 0.95]. In the instance of  $C.A$ , there is no discernible pattern for the pre-trained 2D UNet, which gives values around 0.7 for all  $N$ . This is in contrast to the 3D UNet’s behavior, which exhibits increasing values of the  $F_1$  score (from 0.53 to 0.75) as  $N$  increases.

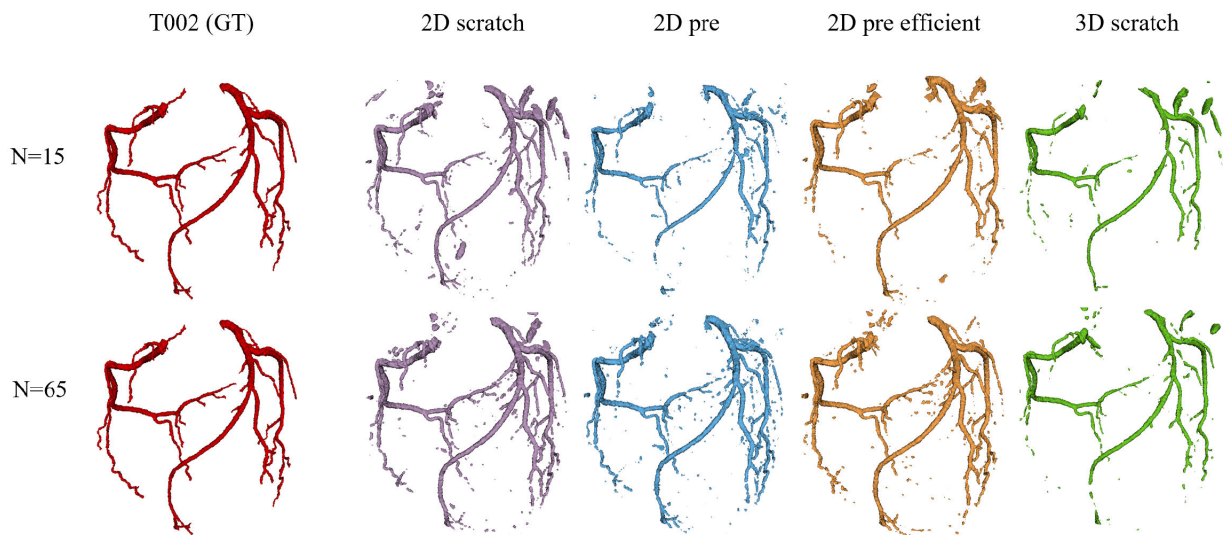
In Fig. 5.B, the  $F_1$  score values are shown when only the  $FPs$  that are attached to the vessel are taken into account. These results do not show a different pattern with respect to Fig. 5.A, but they do show an increase of up to 0.2.

The Recall and Precision metrics are given to provide a more precise picture of the network’s performance. Recall





**FIGURE 8.** Segmentation prediction for test patient T002 with networks trained with aorta and coronary arteries ( $A + C.A$ ).



**FIGURE 9.** Segmentation prediction for test patient T002 with networks trained with coronary arteries only ( $C.A$ ).

tells us how much of the cardiac tree has been recognised by the network. Fig. 5.C displays the outcomes. The same pattern is found for both networks, an increased trend with  $N$  in general and a superior outcome with 2D pretrained UNet. We also notice the “aorta effect” (this refers to the fact that the aorta is a large structure easily recognisable by the network), having recall values greater than 0.8 when training  $A + C.A$ .

To avoid the “aorta effect” Fig. 5.D displays the Recall values in the coronary arteries regardless of whether the trained structure is  $A + C.A$  or  $C.A$ . The positive dependence

on  $N$  can be demonstrated for all eventualities in this case. Mean values for the pre-trained 2D UNet with  $A + C.A$  start at 0.57 when  $N = 15$  and rise sharply when  $N > 35$ , reaching 0.93 when  $N = 65$ . When  $N \leq 35$ , this identical network trained for  $C.A$  exhibits values that are roughly 10% higher than for  $A + C.A$ ; for bigger values of  $N$ , it follows an upward trend, reaching a mean value of 0.82 when  $N = 65$ . Furthermore, when  $N > 35$ , training  $A + C.A$  produces higher outcomes than  $C.A$ .

The 3D UNet pattern is similar, albeit the Recall value is lower than in the pre-trained 2D pattern. When training with

the entire structure ( $A + C.A$ ), there is a certain amount of stalling around 0.5 when  $N \in [25, 45]$ . When  $N = 55$ , however, this value is exceeded until it reaches 0.62. We can see a growing trend for  $C.A$  until  $N = 55$ , when values stabilise.

Furthermore, the network's Precision is displayed in 5.E. In the case of pre-trained 2D UNet with  $A + C.A$ , a diminishing trend with rising  $N$  is observed (though it always remains greater than 0.8). This is due to the rise in  $FP$  (Fig. 5.F). When training  $C.A$ , the same thing happens, but the mean values remain in the range [0.66, 0.8].

This contrasts with the stable mean values around [0.96, 0.98] of the 3D UNet  $A + C.A$ . In the case of the  $C.A$ , an ascending pattern of accuracy is observed up to  $N = 45$  with a value of 0.84.

The number of connected components in the coronary arteries was also counted. Figure 5.G displays the number of connected components decreasing as  $N$  increases. When  $N > 35$ , the pre-trained 2D UNet for  $A + C.A$  undergoes an abrupt change, as we go from  $CC > 80$  to  $CC < 40$ . Indeed, this is the first occasion that fewer connected components are obtained than with  $C.A$ . The value of  $C.A$  falls but remains within the range [50, 70]. The 3D network, on the other hand, displays values below 50 with  $N < 45$  and only surpasses  $CC = 50$  with  $N = 55$ . With  $N = 65$ , the 3D network with  $C.A$  maintaining steady values around  $CC = 30$  and climbing to  $CC = 46$ .

For this particular parameter, the result with post-processing  $IG$  (post-processing  $GI$  shows a similar result in this case) for  $N = 65$  is also included. Note that, the number of connected components is largely reduced, bringing us below 15. For the rest of the parameters, the results with the post-processing are not shown as they do not suffer a significant variation with respect to the original ones. However, they can be seen in Fig. S6 and Fig. S7 in Supplementary Material.









## B. COMPARISON WITH OTHER NETWORKS

Fig. 8 and Fig. 9 illustrate the prediction of the 4 networks (2D UNet from scratch, 2D pre-trained UNet, 2D pre-trained EfficientUNet and 3D UNet) for test patient T002, for  $A + CA$  and  $C.A$  only, respectively. Similar figures for test patients T005, T006 y T007 are in Fig. S8 to Fig. S13 in Supplementary Material.

The bar charts and concrete value of the parameters can be found in Fig. S14 and Fig. S15 and the parameters table Supplementary Material, respectively.

When the number of data available is limited ( $N = 15$ ), the recognition of  $A + C.A$  geometry for 2D without pre-training becomes particularly difficult. It manages to recognise part of the aorta and coronary arteries but does not distinguish them from other bright structures such as ribs or myocardium. However, the pre-trained networks (2D pre-trained UNet and pre-trained EfficientUNet) show complete and clean geometries (absence of false positives), rising its  $F_1$  score

**TABLE 1.** Comparison of results between the segmentation predicted by the corresponding network and the manual segmentation for *lesion1*. The first row shows the difference between the network volume and the manual segmentation volume, the second row shows the percentage of volume at the intersection over the manual segmentation volume, the third, fourth and fifth rows show DSC, precision and recall parameters, respectively, between the network volume and the manual segmentation volume. Yellow shows the manual segmentation (ground truth) and blue shows the AI result. The corresponding networks are 2D UNet pre-trained and 3D UNet, trained with  $N = 65$ , for aorta and coronary arteries ( $A + C.A$ ) and coronary arteries alone ( $C.A$ ).

Lesion 1	2D pre ( $A + C.A$ )	3D ( $A + C.A$ )	2D pre ( $C.A$ )	3D ( $C.A$ )
Volume difference ( $mm^3$ )	5.04	-4.10	5.18	-21.62
Net overlap	88.70%	86.94%	90%	61.74%
DSC	0.85	0.90	0.86	0.75
Precision	0.82	0.93	0.83	0.97
Recall	0.89	0.87	0.90	0.62
Front view				
Side view				

to 0.9. In particular, the EfficientUNet has all major vessels complete.

The 3D UNet shows a similar behaviour to that of the 2D UNet, with partial structure recognition. Nevertheless, it has an accuracy value around 0.9, as opposed to  $< 0.2$  for the 2D UNet. This implies that the structures it recognises are indeed the ones of interest.

On the other hand, when the number of patients is high ( $N = 65$ ), the 4 networks show similar results. Even the 2D from scratch is competitive with the pre-trained ones, improving by 5% the results of the 2D pre-trained UNet, in terms of precision and recall. It also shows more connected vessels. On the other hand, the 3D UNet stands out for its low number of false positives and precision.





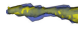

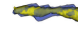

The training for  $C.A$  shows a different behaviour, even with  $N = 15$ , all networks are able to recognise the main vessels ( $F_1 > 0.6$ ). Increasing the number of patients to  $N=65$  reduces the number of false positives and recognises vessels with higher accuracy and connectivity.

## C. STENOSIS PREDICTION

Expert cardiologists determined the accuracy of stenosis segmentation for two calcium-free lesions. Fig. 6 and Fig. 7 show the lesion location and prediction of the neural networks (2D pre-trained UNet and 3D UNet) for  $N = 65$ . The most severe lesion is *lesion1* (Fig. 6).

Table 1 shows a comparison of the manual segmentation of the first lesion. As shown, all training types successfully identify the lesion, with the exception of 3D UNet  $C.A$ , that cuts the vessel at its narrowest point. The lesion is overestimated by the pre-trained 2D UNet.

**TABLE 2.** Comparison of results between the segmentation predicted by the corresponding network and the manual segmentation for *lesion2*. The first row shows the difference between the network volume and the manual segmentation volume, the second row shows the percentage of volume at the intersection over the manual segmentation volume, the third, fourth and fifth rows show DSC, precision and recall parameters, respectively, between the network volume and the manual segmentation volume. Yellow shows the manual segmentation (ground truth) and blue shows the AI result. The corresponding networks are 2D UNet pre-trained and 3D UNet, trained with  $N = 65$ , for aorta and coronary arteries ( $A + C.A.$ ) and coronary arteries alone ( $C.A.$ ).

Lesion 2	2D pre ( $A + C.A.$ )	3D ( $A + C.A.$ )	2D pre ( $C.A.$ )	3D ( $C.A.$ )
Volume difference ( $mm^3$ )	8.80	2.86	10.61	4.68
Net overlap	95.53%	86.58%	93.75%	88.22%
DSC	0.79	0.81	0.77	0.80
Precision	0.68	0.77	0.64	0.74
Recall	0.95	0.87	0.94	0.88
Front view				
Side view				

In the case of *lesion2*, the findings are shown in Table 2. The pre-trained 2D UNet overestimates the lesion region significantly, which lowers the DSC below 0.8.

#### D. LOSS FUNCTION

In the field of medical image segmentation, loss functions are usually based on cross entropy or the dice coefficient [36], [40], [41]. In this study, a test was performed to see the behaviour of the 2D pre-trained UNet with the loss function dice coefficient ( $N = 65$  and  $A + C.A.$ ). This implementation did not generate significantly better results in the geometry of interest. However, it does show a reduction in the number of false positives in agreement with [40] and [41]. (See Fig. S28 and Table S1 for details).

#### IV. DISCUSSION AND CONCLUSION

The way in which this article addresses the challenges exposed in the Introduction (Section I) can be summarised as follows:

- 1) The lack of data, inherent to these type of studies, is considered and its effect analysed by studying the variation of the network performance as the number of data considered is increased.
- 2) Class imbalance is mitigated by focal loss. That is, more importance is given to the error in the vessel class than in the background class.
- 3) A comparison is made between the performance of a network with a very low computational cost, a 2D UNet with a pre-trained encoder in ImageNet [24], and a network with a high computational cost, a 3D UNet. In addition, in the comparative study, a 2D UNet without pre-training and an EfficientUNet are included to demonstrate the power of this architecture for the segmentation of coronary structures. Note that this manuscript is not intended to be a full

comparison with all the architectures available but, rather, a demonstration that coronary tree segmentation is accessible with these architectures and the suitability of each one.

2D and 3D UNet exhibit outstanding and competitive outcomes in comparison to those published to date. Our technique yields  $F_1$  score (DSC) values of more than 93% for both 2D and 3D UNet in  $A + C.A.$  and 75% in  $C.A.$  (versus 91.20% and 88.80% [12]). It should be emphasised that very detailed segmentations are used for both training and testing in the current study, which may result in lower  $F_1$  score values in  $C.A.$  due to the difficulty in segmenting thin and distal vessels. Nevertheless, the results produced very detailed coronary structures with high applicability in the cardiology field.

The 2D UNet with a pre-trained encoder and millions of images exhibits less volatility in the parameter values as the number of patients increases. In reality, it is already possible to reproduce a coronary tree with a small set of data ( $N = 15$ ). This contrasts with the 2D UNet from scratch, which with a low number of patients fails to reproduce the basic structures ( $A + C.A.$ ). Despite its cheap computational cost, it is thus an architecture with considerable potential. The influence of different backbones has also been highlighted. In our case, with the same configuration, the 2D EfficientUNet shows less overestimated and more connected vessels than the 2D pre-trained UNet.

The 3D UNet, on the other hand, is more dependent on the number of training data and exhibits cleaner and more connected components structures despite not recognising as many distal vessels.

Furthermore, we show the effect of increasing the size of the training data set. In terms of structure recognition, we observe a positive dependence in the 2D UNet case. However, the number of false positives rises. This is not a major issue because the majority of them are not attached to the vessels and can be easily removed in the postprocessing. It is also noticed that after training using  $C.A.$ , the number of false positives is lower, which is consistent with [12]. It is probable that reducing the focal loss impact as  $N$  increases aids in noise removal. Reduction in the number of false positives can also be achieved by modifying the cost function. This has been tested with the dice coefficient and a reduction of up to an order of magnitude in  $FP$  has been observed. However, it also leads to a decrease in prediction accuracy in vessels.

In addition, an evaluation of the algorithms for the detection of lesions (stenosis) is also made. Although both approaches recognise the presence of lesions, it has been observed that 2D UNet overestimates more. In the case of the 3D UNet, training using  $A + C.A.$  results in higher accuracy. As a consequence, the computationally intensive strategy is the more accurate in terms of lesions.

The limitations of this study include the time-consuming effort of collecting and segmenting patients, as well as the subjectivity introduced by the expert performing the



segmentation. Furthermore, the lack of a database and code makes comparison with other studies challenging.

In summary, it has been demonstrated that artificial intelligence can be a very useful tool for clinical care and diagnosis. This provides the possibility of using a user-independent, fast and accurate method. Furthermore, the use of transfer learning for CCTA is a novelty and allows faster training with less data, while maintaining a certain quality in the segmentation. This is of great importance when working with medical imaging, and especially CT, as images are difficult to segment manually. Future work could incorporate transfer learning in the case of a 3D UNet, which is difficult to perform due to data scarcity, as well as calcified lesions.

## ACKNOWLEDGMENT

The simulations were run in the Supercomputer Center of Galicia (CESGA) and the authors acknowledge their support.

## REFERENCES

- [1] World Health Organization. *The Top 10 Causes of Death*. Accessed: Jun. 6, 2022. [Online]. Available: <https://www.who.int/news-room/fact-sheets/detail/the-top-10-causes-of-death>
- [2] R. D. Shahjehan and B. S. Bhutta, "Coronary artery disease," in *StatPearls*. Treasure Island, FL, USA: StatPearls Publishing, Jan. 2023.
- [3] U. J. Schoepf, C. R. Becker, B. M. Ohnesorge, and E. K. Yucel, "CT of coronary artery disease," *Radiology*, vol. 232, pp. 18–37, Jul. 2004.
- [4] L. Yang, P. P. Xu, U. J. Schoepf, C. Tesche, B. Pillai, R. H. Savage, C. X. Tang, F. Zhou, H. D. Wei, Z. Q. Luo, Q. G. Wang, C. S. Zhou, M. J. Lu, G. M. Lu, and L. J. Zhang, "Serial coronary CT angiography-derived fractional flow reserve and plaque progression can predict long-term outcomes of coronary artery disease," *Eur. Radiol.*, vol. 31, no. 9, pp. 7110–7120, Feb. 2021.
- [5] A. Otero-Cacho, D. López-Otero, M. I. Villa, B. Díaz-Fernández, M. Bastos-Fernández, A. García-Campos, V. Pérez-Muñuzuri, A. P. Muñuzuri, and R. González-Juanatey, "Non-invasive assessment of coronary lesions by computer tomography fractional flow reserve compared to the invasive technique under hyperaemic and basal conditions," *Cardioclinics*, 2023.
- [6] A. Kurata, N. Fukuyama, K. Hirai, N. Kawaguchi, Y. Tanabe, H. Okayama, S. Shigemi, K. Watanabe, T. Uetani, S. Ikeda, S. Inaba, T. Kido, T. Itoh, and T. Mochizuki, "On-site computed tomography-derived fractional flow reserve using a machine-learning algorithm—Clinical effectiveness in a retrospective multicenter cohort," *Circulat. J.*, vol. 83, no. 7, pp. 1563–1571, 2019.
- [7] Z. Gao, X. Wang, S. Sun, D. Wu, J. Bai, Y. Yin, X. Liu, H. Zhang, and V. H. C. de Albuquerque, "Learning physical properties in complex visual scenes: An intelligent machine for perceiving blood flow dynamics from static CT angiography imaging," *Neural Netw.*, vol. 123, pp. 82–93, Mar. 2020.
- [8] A. Esteva, A. Robicquet, B. Ramsundar, V. Kuleshov, M. DePristo, K. Chou, C. Cui, G. Corrado, S. Thrun, and J. Dean, "A guide to deep learning in healthcare," *Nature Med.*, vol. 25, no. 1, pp. 24–29, Jan. 2019.
- [9] A. Lin, M. Kolossváry, M. Motwani, I. Išgum, P. Maurovich-Horvat, P. J. Slomka, and D. Dey, "Artificial intelligence in cardiovascular CT: Current status and future implications," *J. Cardiovascular Comput. Tomogr.*, vol. 15, no. 6, pp. 462–469, Nov. 2021.
- [10] O. Ronneberger, P. Fischer, and T. Brox, "U-Net: Convolutional networks for biomedical image segmentation," in *Proc. Int. Conf. Med. Image Comput. Comput.-Assist. Intervent.*, 2015, pp. 234–241.
- [11] A. G. Blaiech, A. Mansour, A. Kerkeni, M. H. Bedoui, and A. B. Abdallah, "Impact of enhancement for coronary artery segmentation based on deep learning neural network," in *Pattern Recognition and Image Analysis*. Cham, Switzerland: Springer, 2019, pp. 260–272.
- [12] W. K. Cheung, R. Bell, A. Nair, L. J. Menezes, R. Patel, S. Wan, K. Chou, J. Chen, R. Torii, R. H. Davies, J. C. Moon, D. C. Alexander, and J. Jacob, "A computationally efficient approach to segmentation of the aorta and coronary arteries using deep learning," *IEEE Access*, vol. 9, pp. 108873–108888, 2021.
- [13] L.-S. Pan, C.-W. Li, S.-F. Su, S.-Y. Tay, Q.-V. Tran, and W. P. Chan, "Coronary artery segmentation under class imbalance using a U-Net based architecture on computed tomography angiography images," *Sci. Rep.*, vol. 11, no. 1, p. 14493, Jul. 2021.
- [14] W. Huang, L. Huang, Z. Lin, S. Huang, Y. Chi, J. Zhou, J. Zhang, R. Tan, and L. Zhong, "Coronary artery segmentation by deep learning neural networks on computed tomographic coronary angiographic images," in *Proc. 40th Annu. Int. Conf. IEEE Eng. Med. Biol. Soc. (EMBC)*, Jul. 2018, pp. 608–611.
- [15] L. Gu and X.-C. Cai, "Fusing 2D and 3D convolutional neural networks for the segmentation of aorta and coronary arteries from CT images," *Artif. Intell. Med.*, vol. 121, Nov. 2021, Art. no. 102189.
- [16] F. Tian, Y. Gao, Z. Fang, and J. Gu, "Automatic coronary artery segmentation algorithm based on deep learning and digital image processing," *Appl. Intell.*, vol. 51, no. 12, pp. 8881–8895, Apr. 2021.
- [17] L. R. Dice, "Measures of the amount of ecologic association between species," *Ecology*, vol. 26, no. 3, pp. 297–302, Jul. 1945.
- [18] Y. Duan, J. Feng, J. Lu, and J. Zhou, "Context aware 3D fully convolutional networks for coronary artery segmentation," in *Statistical Atlases and Computational Models of the Heart. Atrial Segmentation and LV Quantification Challenges*. Granada, Spain: Springer, 2019, pp. 85–93.
- [19] H. Azizpour, A. S. Razavian, J. Sullivan, A. Maki, and S. Carlsson, "From generic to specific deep representations for visual recognition," in *Proc. IEEE Conf. Comput. Vis. Pattern Recognit. Workshops*, Jun. 2015, pp. 36–45.
- [20] N. Jávorszky, B. Homonnay, G. Gerstenblith, D. Bluemke, P. Kiss, M. Török, D. Celentano, H. Lai, S. Lai, and M. Kolossváry, "Deep learning-based atherosclerotic coronary plaque segmentation on coronary CT angiography," *Eur. Radiol.*, vol. 32, no. 10, pp. 7217–7226, May 2022.
- [21] E. Ovalle-Magallanes, J. G. Avina-Cervantes, I. Cruz-Aceves, and J. Ruiz-Pinales, "Transfer learning for stenosis detection in X-ray coronary angiography," *Mathematics*, vol. 8, no. 9, p. 1510, Sep. 2020.
- [22] S. Candemir, R. D. White, M. Demirel, V. Gupta, M. T. Bigelow, L. M. Prevedello, and B. S. Erdal, "Automated coronary artery atherosclerosis detection and weakly supervised localization on coronary CT angiography with a deep 3-dimensional convolutional neural network," *Computerized Med. Imag. Graph.*, vol. 83, Jul. 2020, Art. no. 101721.
- [23] K. Simonyan and A. Zisserman, "Very deep convolutional networks for large-scale image recognition," 2014, *arXiv:1409.1556*.
- [24] A. Krizhevsky, I. Sutskever, and G. E. Hinton, "ImageNet classification with deep convolutional neural networks," in *Proc. Adv. Neural Inf. Process. Syst.*, vol. 25, 2012, pp. 1–9.
- [25] S. Abbara, P. Blanke, C. D. Maroules, M. Cheezum, A. D. Choi, B. K. Han, M. Marwan, C. Naoum, B. L. Norgaard, R. Rubinshtein, P. Schoenhagen, T. Villines, and J. Leipsic, "SCCT guidelines for the performance and acquisition of coronary computed tomographic angiography: A report of the society of cardiovascular computed tomography guidelines committee: Endorsed by the North American society for cardiovascular imaging (NASCI)," *J. Cardiovascular Comput. Tomogr.*, vol. 10, no. 6, pp. 435–449, Nov. 2016.
- [26] R. Kikinis, S. D. Pieper, and K. G. Vosburgh, "3D slicer: A platform for subject-specific image analysis, visualization, and clinical support," in *Intraoperative Imaging and Image-Guided Therapy*, Nov. 2013.
- [27] A. Fedorov et al., "3D slicer as an image computing platform for the quantitative imaging network," *Magn. Reson. Imag.*, vol. 30, no. 9, pp. 1323–1341, 2012.
- [28] A. G. Howard, M. Zhu, B. Chen, D. Kalenichenko, W. Wang, T. Weyand, M. Andreetto, and H. Adam, "MobileNets: Efficient convolutional neural networks for mobile vision applications," 2017, *arXiv:1704.04861*.
- [29] M. Abadi. (2015). *TensorFlow: Large-Scale Machine Learning on Heterogeneous Systems*. [Online]. Available: <https://tensorflow.org>
- [30] M. Tan and Q. Le, "EfficientNet: Rethinking model scaling for convolutional neural networks," in *Proc. Int. Conf. Mach. Learn.*, 2019, pp. 6105–6114.
- [31] P. Iakubovskii. (2019). *Segmentation Models*. [Online]. Available: [https://github.com/qubvel/segmentation\\_models](https://github.com/qubvel/segmentation_models)
- [32] G. Van Rossum and F. L. Drake, *Python 3 Reference Manual*. Scotts Valley, CA, USA: CreateSpace, 2009.
- [33] Python. *Python 3.7.0*. Accessed: Jul. 22, 2022. [Online]. Available: <https://www.python.org/downloads/release/python-370/>
- [34] F. Chollet, "Keras," Tech. Rep., 2015.



- [35] F. Chollet. *Keras Losses*. Accessed: Jul. 22, 2022. [Online]. Available: <https://github.com/keras-team/keras/blob/master/keras/losses.py>
- [36] J. Ma, J. Chen, M. Ng, R. Huang, Y. Li, C. Li, X. Yang, and A. L. Martel, "Loss Odyssey in medical image segmentation," *Med. Image Anal.*, vol. 71, Jul. 2021, Art. no. 102035.
- [37] F. Chollet. *Keras adam optimizer*. Accessed: Jul. 22, 2022. [Online]. Available: [https://github.com/keras-team/keras/blob/master/keras/optimizers/optimizer\\_v2/adam.py](https://github.com/keras-team/keras/blob/master/keras/optimizers/optimizer_v2/adam.py)
- [38] S. Moccia, E. De Momi, S. El Hadji, and L. S. Mattos, "Blood vessel segmentation algorithms—Review of methods, datasets and evaluation metrics," *Comput. Methods Programs Biomed.*, vol. 158, pp. 71–91, May 2018.
- [39] W. Wu, J. Zhang, H. Xie, Y. Zhao, S. Zhang, and L. Gu, "Automatic detection of coronary artery stenosis by convolutional neural network with temporal constraint," *Comput. Biol. Med.*, vol. 118, Mar. 2020, Art. no. 103657.
- [40] B. Liu, J. Dolz, A. Galdran, R. Kobbi, and I. Ben Ayed, "The hidden label-marginal biases of segmentation losses," 2021, *arXiv:2104.08717*.
- [41] S. R. Hashemi, S. S. Mohseni Salehi, D. Erdogmus, S. P. Prabhu, S. K. Warfield, and A. Gholipour, "Asymmetric loss functions and deep densely-connected networks for highly-imbalanced medical image segmentation: Application to multiple sclerosis lesion detection," *IEEE Access*, vol. 7, pp. 1721–1735, 2019.



**BELÉN SERRANO-ANTÓN** was born in Segovia, Spain. She received the dual B.S. degree in mathematics and computer science from the Complutense University of Madrid, Spain, in 2021, and the M.S. degree in computational biology from the Technical University of Madrid, Spain, in 2022. She is currently pursuing the Ph.D. degree with the University of Santiago de Compostela, Spain.

In 2022, she was a Research and Development Engineer with FlowReserve Labs S.L. Her research interests include the application of computer science and mathematical modeling to the biological and clinical fields.



**ALBERTO OTERO-CACHO** received the Ph.D. degree in physics and the M.B.A. degree. He is currently a CSO of FlowReserve Labs S.L. He is also a Civil Engineer. He has developed his professional activity in project management and the application of CFD techniques to the resolution of flow in the circulatory and coronary systems.



**DIEGO LÓPEZ-OTERO** received the Ph.D. degree in health sciences and biomedicine from the University of Santiago de Compostela, Spain. He is currently a Cardiologist with Hospital Clínico Universitario de Santiago de Compostela (CHUS), Spain. He is the author of more than 50 scientific articles in national and international journals of the first quartile in the cardiovascular area. He is an editor of two books and the author of numerous book chapters.



**BRAIS DÍAZ-FERNÁNDEZ** received the degree in medicine and surgery from the University of Santiago de Compostela and the master's degree in statistics in health sciences from the Autonomous University of Barcelona. He is currently a Cardiologist with Hospital Clínico Universitario de Santiago de Compostela (CHUS).



**MARÍA BASTOS-FERNÁNDEZ** received the master's degree in clinical research, the master's degree in diagnostic imaging in cardiology, and the degree in medicine and surgery. She is currently a Cardiologist and an Expert in cardiac imaging with the Department of Cardiology and Cardiac Intensive Care, Hospital Clínico Universitario de Santiago de Compostela (CHUS), Spain.



**VICENTE PÉREZ-MUÑUZURI** was the Director of Meteogalicia (regional meteorological service dependent of Xunta de Galicia), from 1999 to 2014. He is currently a Full Professor with the University of Santiago de Compostela (USC). He is also the current Vice-Rector of Research and Innovation with USC. He has edited three books, and two special issues of an international journal, and has published more than 130 articles in international journals (JCR),

in addition to giving more than 100 conferences.



**JOSÉ RAMÓN GONZÁLEZ-JUANATEY** was the President of the Spanish Society of Cardiology, from 2013 to 2015, and an Advisor for cardiovascular health to the Ministry of Health, from 2017 to 2019. He is currently a Full Professor with the University of Santiago de Compostela, Spain, and the Director of the Cardiology Research Group, Instituto de Investigación Sanitaria de Santiago de Compostela (IDIS). He is a principal investigator in important international clinical trials in cardiology. He has participated in more than 300 publications in international journals, such as *The New England Journal of Medicine*, *The Lancet*, *JAMA*, *Circulation*, and *European Heart Journal*.



**ALBERTO P. MUÑUZURI** is currently a Professor of physics with the University of Santiago de Compostela, Spain, and the Director of the Nonlinear Physics Group. He has supervised nine Ph.D. theses and numerous master's theses and has been a principal investigator of more than ten research projects in competitive calls during the last 12 years. He has more than 120 articles published in international journals, including several *PRL*, *PNAS*, *Nature Communications*, and

*Scientific Reports*, approximately 40 conferences in international congresses, 20 seminars given in different universities, and 30 stays in universities in different countries.

• • •